THE WIDTH OF NEUTRON SPECTRA AND THE HEAT MODE OF FLUIDS

I.M. DE SCHEPPER, E.G.D. COHEN [1]
Interuniversitair Reactor Instituut, 2629 JB Delft, The Netherlands

and

M.J. ZUILHOF
Instituut voor Theoretische Fysica, Rijksuniversiteit Utrecht, 3508 TA Utrecht, The Netherlands

Received 15 February 1984

The width of neutron spectra is studied on the basis of kinetic theory as a function of wavenumber and density and appears to be determined by the heat mode of the fluid. For high-density fluids an interference of static and dynamic effects in this mode is observed.

In two previous publications, the dominant eigenmodes of a hard-sphere fluid were approximately determined on the basis of kinetic theory [1,2]. Thus, the extensions of the five hydrodynamic modes, as well as the self-diffusion mode to large wavenumbers were included in these calculations. It appeared that like in hydrodynamics the (extended) heat mode determined both the width and the height of the neutron spectrum $S(k, \omega)$ as a function of frequency ω for a large range of wavenumbers k. In particular, it was shown that the so-called de Gennes narrowing of $S(k, \omega)$ at high densities is due to a considerable softening of the heat mode eigenvalue $z_h(k)$ which becomes diffusion-like at about $k\sigma \approx 2\pi$ where σ is the hard-sphere diameter. A comparison with neutron scattering data for liquid argon [3] and rubidium [4] showed that the heat mode also dominates $S(k, \omega)$ for these fluids.

In this letter, we report new results for $z_h(k)$, which were computed from the generalized Enskog theory for a much wider range of densities and wavenumbers and in a much higher approximation than before. We will compare these results with recent molecular dynamics (MD) data for hard spheres [5,6] as well as neutron scattering data for liquid helium [7], argon [8,9] and krypton [10].

We consider the inhomogeneous generalized Enskog operator $L(\boldsymbol{k})$ that governs the time evolution of the correlation functions in a fluid of hard spheres:

$$L(\boldsymbol{k}) = -\mathrm{i}\boldsymbol{k}\cdot\boldsymbol{v} + ng(\sigma)\,\Lambda_{\boldsymbol{k}} + nA_{\boldsymbol{k}}, \tag{1}$$

where $\boldsymbol{k}$ is a wave vector, $\boldsymbol{v}$ the velocity, $g(\sigma)$ the radial distribution for two spheres at contact, n the number density and $\Lambda_{\boldsymbol{k}}$ a binary collision operator defined on a function $h(\boldsymbol{v})$ by

$$\Lambda_{\boldsymbol{k}} h(\boldsymbol{v}) = -\sigma^2 \int \mathrm{d}\hat{\sigma} \int \mathrm{d}\boldsymbol{v}'\, \phi(v')\, \boldsymbol{g}\cdot\hat{\sigma}\, \theta(\boldsymbol{g}\cdot\hat{\sigma})$$

$$\times \{h(\boldsymbol{v}) - h(\boldsymbol{v}^*) + \mathrm{e}^{-\mathrm{i}\boldsymbol{k}\cdot\hat{\sigma}\sigma}[h(\boldsymbol{v}') - h(\boldsymbol{v}'^*)]\},$$

while the mean field operator $A_{\boldsymbol{k}}$, which contains the static correlations in the fluid, is defined by

$$A_{\boldsymbol{k}} h(\boldsymbol{v}) = [C(k) - g(\sigma)\, C_0(k)]$$

$$\times \int \mathrm{d}\boldsymbol{v}'\, \phi(v')\, \mathrm{i}\boldsymbol{k}\cdot\boldsymbol{v}' h(\boldsymbol{v}').$$

Here $\hat{\sigma}$ is a unit vector, $\boldsymbol{g} = \boldsymbol{v} - \boldsymbol{v}'$, $\theta(x)$ the unit step function, $\boldsymbol{v}^* = \boldsymbol{v} - \boldsymbol{g}\cdot\hat{\sigma}\hat{\sigma}$ and $\boldsymbol{v}'^* = \boldsymbol{v}' + \boldsymbol{g}\cdot\hat{\sigma}\hat{\sigma}$ are the velocities of the restituting collision, $C(k) = n^{-1}$ [1 $- 1/S(k)$] and $C_0(k)$ the low-density limit of the di-

[1] Permanent address: The Rockefeller University, 1230 York Avenue, New York, NY 10021, USA.

0.375-9601/84/$ 03.00

rect correlation function $C(k)$, with $S(k)$ the static structure factor, $\phi(v) = (\beta M/2\pi)^{3/2} \exp(-\beta M v^2/2)$, where M is the mass of the hard sphere and $\beta = 1/k_B T$ with T the temperature and k_B Boltzmann's constant. The heat mode appears as a particular term in the spectral decomposition of $L(\boldsymbol{k})$,

$$L(\boldsymbol{k}) = -\sum_j |\Psi_j(\boldsymbol{k}, \boldsymbol{v})\rangle z_j(k) \langle\Phi_j(\boldsymbol{k}, \boldsymbol{v})|, \tag{2}$$

where each $z_j(k)$ denotes an eigenvalue of $-L(\boldsymbol{k})$ and $\Psi_j(\boldsymbol{k}, \boldsymbol{v})$ and $\Phi_j(\boldsymbol{k}, \boldsymbol{v})$ are the corresponding right and left eigenfunctions. The bracket notation in eq. (2) refers to the inner product $\langle f|g\rangle = \langle f^* g\rangle = \int d\boldsymbol{v}\, \phi(v) f^* g$. With eqs. (1, 2) one has [2]

$$S(k, \omega) = \pi^{-1} S(k)\, \mathrm{Re}\, \langle 1/[\mathrm{i}\omega - L(\boldsymbol{k})]^{-1}\rangle$$

$$= \pi^{-1} S(k)\, \mathrm{Re} \sum_j \frac{A_j(k)}{\mathrm{i}\omega + z_j(k)}, \tag{3}$$

where $A_j(k) = \langle \Psi_j(\boldsymbol{k}, \boldsymbol{v})\rangle \langle \Phi_j^*(\boldsymbol{k}, \boldsymbol{v})\rangle$. To determine $z_h(k)$ explicitly, $\Lambda_{\boldsymbol{k}}$ in eq. (1) is approximated by operators $\Lambda_{\boldsymbol{k}}^{(N)}$ labeled with N and given by

$$\Lambda_{\boldsymbol{k}}^{(N)} = \sum_{j,l=1}^{N-1} |\phi_j\rangle\langle\phi_j^*\, \Lambda_{\boldsymbol{k}}\, \phi_l\rangle\langle\phi_l|$$

$$+ \langle\phi_N^*\, \Lambda_{\boldsymbol{k}}\, \phi_N\rangle (1 - P_{N-1}). \tag{4}$$

Here P_N projects on $\phi_1, \ldots, \phi_N$ and $\{\phi_j\}$ is the complete set of orthonormal polynomials in $\boldsymbol{v}$ given by

$$N_{r,l} v^l L_r^{(l+1/2)}(\beta M v^2/2)\, Y_l^{(m)}(\boldsymbol{v}/v),$$

labeled by the "quantum numbers" $(r, l, m) = j$, where the $L_r^{(l+1/2)}$ are associated Laguerre polynomials with normalization constants $N_{r,l}$, and the $Y_l^{(m)}$ are spherical harmonics with the z axis taken in the $\boldsymbol{k}$ direction. The cylindrical symmetry of $L(\boldsymbol{k})$ around the $\boldsymbol{k}$ axis implies that the eigenfunctions in eq. (2) can all be labeled by m. For the heat mode $m = 0$ and we included the 11 polynomials with $m = 0$ and (r, l) equal to (0, 0); (0, 1); (1, 0); (1, 1); (0, 2); (2, 0); (2, 1); (1, 2); (3, 0); (0, 3); and (2, 2). Using then the methods discussed before [2], $N - 1$ terms on the right-hand side of eq. (2), can be determined explicitly. In particular, a convergent heat mode (j = h) is obtained for the k values considered here.

In addition to $L(\boldsymbol{k})$, the Lorentz–Enskog operator $L^s(\boldsymbol{k}) = -\mathrm{i}\boldsymbol{k}\cdot\boldsymbol{v} + ng(\sigma)\, \Lambda_\infty$, which governs the time evolution of the self-correlation functions in the fluid, is relevant. The operator $\Lambda_\infty = \lim_{k\to\infty} \Lambda_{\boldsymbol{k}}$ and is given by $\Lambda_{\boldsymbol{k}}$ with its last two terms neglected. The spectral decomposition of $L^s(\boldsymbol{k})$ can be determined in a completely similar manner as that of $L(\boldsymbol{k})$ and since $L(\boldsymbol{k})$ tends to $L^s(\boldsymbol{k})$ for large k ($\lim_{k\to\infty} A_{\boldsymbol{k}} = 0$), the eigenmodes of $L(\boldsymbol{k})$ tend to those of $L^s(\boldsymbol{k})$. In particular the heat mode eigenvalue $z_h(k)$ tends to the eigenvalue $z_D(k)$ of the self-diffusion mode of $L^s(k)$. For small k, both agree with hydrodynamics: $z_h(k) = \alpha_E k^2$, $z_D(k) = D_E k^2$ where α_E and D_E are the thermal diffusivity and the self-diffusion coefficient according to the Enskog theory. We note that $S(k, \omega)$ can also be determined directly from the first equality in eq. (3) using eq. (4) for $\Lambda_{\boldsymbol{k}}$, without making a spectral decomposition. The halfwidth $\omega_H(k)$ can be derived in general from the implicit equation $S(k, \omega_H(k)) = \frac{1}{2} S(k, 0)$. We can determine $\omega_H^s(k)$, i.e., the halfwidth of the incoherent scattering function $S_s(k, \omega) = \pi^{-1} \mathrm{Re}\langle[\mathrm{i}\omega - L^s(k)]^{-1}\rangle$, in a completely similar manner. Since $L(\boldsymbol{k})$ approaches $L^s(\boldsymbol{k})$ and $S(k)$ approaches 1, $\omega_H(k)$ tends to $\omega_H^s(k)$ for large k.

The results for $z_h(k)$, $\omega_H(k)$, $z_D(k)$ and $\omega_H^s(k)$ are plotted in figs. 1 and 2 in units t_σ^{-1} as functions of $k\sigma$, for various reduced densities $V_0/V = n\sigma^3/\sqrt{2}$. Here V_0 is the volume of close packing, and $t_\sigma = \sigma(\beta m)^{1/2}/2$, is a time a particle needs to traverse σ with thermal speed.

To interpret our results, we also need the mean free time t_E and the mean free path l_E, where

$$\sigma/l_E = (\pi/2)^{1/2}\, t_\sigma/t_E = 2\pi g(\sigma)\, V_0/V.$$

For each V_0/V the value of the corresponding σ/l_E can be deduced from the arrows in figs. 1 and 2, which point to the values of $k\sigma$ where $kl_E = 1$. Thus for $V_0/V = 0.25, 0.33, 0.53, 0.575$ and 0.625, $\sigma/l_E = 2.64, 4.30, 11.92, 14.97$ and 19.32, respectively.

We first note that $\omega_H^s(k)\, t_E$ and $z_D(k)\, t_E$ as functions of kl_E are independent of the density. For $kl_E < 1$, $z_D(k) \approx D_E k^2$ and strongly dominates $S_s(k, \omega)$ so that $\omega_H^s(k) \approx z_D(k)$ within a few percent (cf. figs. 1 and 2). For $kl_E \lesssim 1$, $\omega_H^s(k)$ and $z_D(k)$ change from a quadratic to a linear behavior in k where the slopes of both are close to that of ω_H^s of an ideal gas. $\omega_H^s(k)$ does *not* approach the ideal-gas limit, however, but differs asymptotically a constant amount from it,

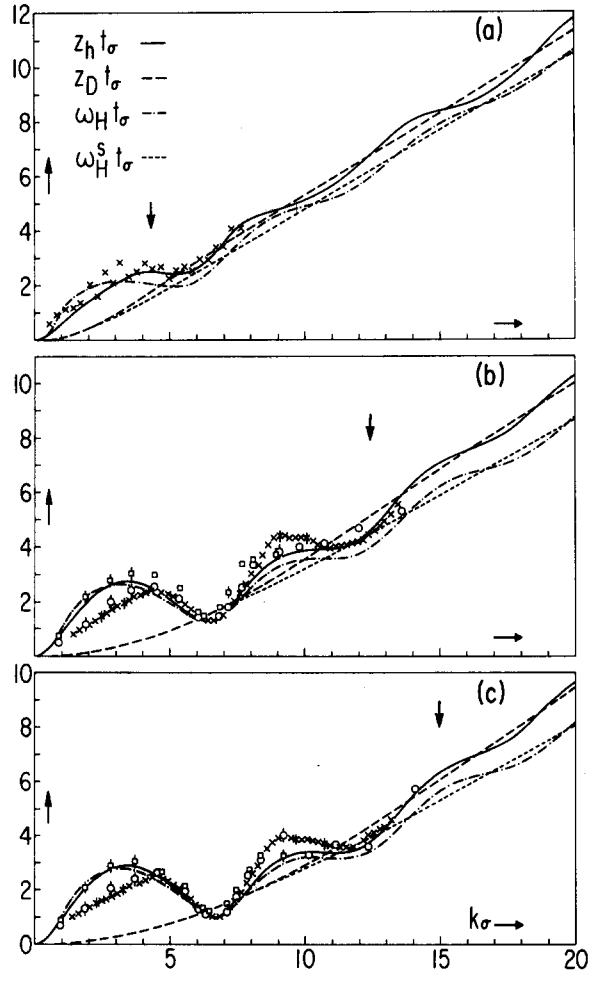

Fig. 1. Comparison of hard-sphere theory with (a) ω_H of liquid He at 4.2 K (x) (σ = 2.92 Å, V_0/V = 0.33); (b) $\omega_H = z_h$ of liquid Ar at 120 K, 115 bar (x) (σ = 3.43Å, V_0/V = 0.53), of a Lennard-Jones (LJ) (○) and of a repulsive Lennard-Jones (RLJ) (□) fluid, discussed in ref. [13]; (c) $\omega_H = z_h$ of liquid Ar at 120 K and 400 bar (σ = 3.43 Å, V_0/V = 0.575), of a LJ (○) and of a RLJ (□) fluid. Typical error bars of experimental or MD points are indicated. The flat arrow points to that value of $k\sigma$ where $kl_E = 1$.

since for large k, $\omega_H^s(k)\, t_E = \frac{1}{2}(\pi \ln 2)^{1/2} kl_E - 0.3310 + O((kl_E)^{-1})$ [11]. This deviation is peculiar for the hard-sphere interaction [12] and should disappear for a realistic interparticle potential when $\omega_H^s > t_s^{-1}$, where t_s is the average time to traverse the steep repulsive part of the potential [11,12]. The growing difference of $z_D(k)$ and $\omega_H^s(k)$ for $kl_E > 1$ is due to the fact that for increasing k other (kinetic) modes increasingly contribute to $\omega_H^s(k)$.

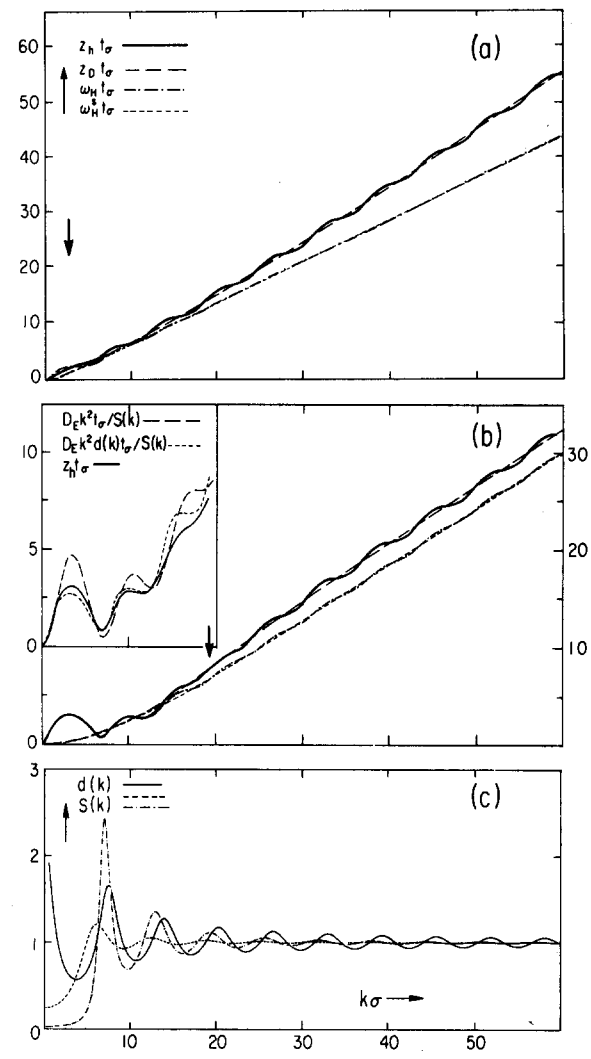

Fig. 2. Eigenmodes and halfwidths as a function of $k\sigma$ for a hard-sphere fluid at V_0/V = 0.25 (a); same for V_0/V = 0.625 (b); $S(k)$ for V_0/V = 0.25 (– – –) and 0.625 (–•–) and $d(k)$ (c). Inset in (b) gives $z_h t_\sigma$ and two approximations discussed in the text as a function of $k\sigma$. The fat arrow points to that value of $k\sigma$ where $kl_E = 1$.

Just as for $z_D(k)$ and $\omega_H^s(k)$, we find that for $kl_E < 1$, $z_h(k)$ dominates $\omega_H(k)$ while the growing difference for $kl_E > 1$ is due to the fact that other modes increasingly contribute to $\omega_H(k)$. In fact, we find that the extended heat and sound modes are sufficient to describe $S(k, \omega)$ – and in particular $\omega_H(k)$ – adequately for $kl_E < 1$, where the influence of the sound modes on $\omega_H(k)$ increases with decreasing den-

sity (cf. figs. 1 and 3a). For the region $1 < kl_E < 2$, three more (kinetic) modes are needed and sufficient to describe $\omega_H(k)$.

For all densities $\omega_H(k)$ and $z_h(k)$ oscillate around $\omega_H^s(k)$ and $z_D(k)$, respectively (cf. figs. 1 and 2). This is due to the oscillatory behavior of both Λ_k around Λ_∞ and of $S(k)$ around 1. The former behavior can be conveniently characterized by the function $d(k) = \langle\phi_2 \Lambda_k^{-1} \phi_2\rangle / \langle\phi_2 \Lambda_\infty^{-1} \phi_2\rangle$, where $\phi_2 = (\beta m)^{1/2} v_z$ (cf. fig. 2). $d(k)$ is a dimensionless function of $k\sigma$ independent of the density. The oscillations in $d(k)$ are due to the factor $\exp(-i\boldsymbol{k}\cdot\hat{\boldsymbol{o}}\sigma)$ in Λ_k and decrease $\sim(k\sigma)^{-1}$ for large k. Since the $S(k)$-oscillations decrease $\sim(k\sigma)^{-2}$, $d(k)$ dominates $S(k)$ for large k at all densities. For smaller values of k, $S(k)$ increasingly dominates $d(k)$, an effect that increases with density (cf. fig. 2).

For densities $V_0 V > 0.30$, a distinct minimum in $\omega_H(k)$ appears at $k = k_G$. With increasing density, this de Gennes minimum in ω_H becomes more and more pronounced (cf. figs. 1 and 2), while k_G approaches k_S, where $S(k)$ has its first maximum (cf. fig. 3). The occurrence of a minimum in $\omega_H(k)$ at high densities is in our theory directly related to that of $z_h(k)$. To understand the latter, we write

$$L(\boldsymbol{k}) = [L_c(\boldsymbol{k}) + ikl_E L_f(\boldsymbol{k})]\, t_E^{-1},$$

where

$$L_c(\boldsymbol{k}) = (\beta M/16\pi\sigma^4)^{1/2}(1-P_1)\,\Lambda_k\,(1-P_1)$$

describes collisions between particles (P_1 projects on $\phi_1 = 1$) and

$$L_f(\boldsymbol{k}) = (\pi/8)^{1/2}[nC(k)|\phi_1\rangle\langle\phi_2| - \phi_2],$$

incorporates the free streaming as well as the mean field term in eq. (1). $L_c(\boldsymbol{k})$ and $L_f(\boldsymbol{k})$ are both dimensionless, depend only on $k\sigma$ and are of order 1 for all k. Thus, as long as $kl_E < 1$, L_f can be treated as a perturbation to L_c. To second order in kl_E, one finds then for the heat mode

$$z_h(k) = [D_E k^2/S(k)]\, d(k) + O((kl_E)^4), \qquad (5)$$

which applies to the region $0 < k\sigma < \sigma/l_E$ (i.e., $kl_E < 1$), where $k\sigma = 0$ is excluded since $L_c(\boldsymbol{k})$ has a fivefold degenerate zero eigenvalue at $k = 0$ and nondegenerate perturbation theory has been applied to obtain eq. (5). For densities $V_0/V \gtrsim 0.52$, $k_G\sigma = 2\pi$, which is well within the region where $kl_E < 1$, so that

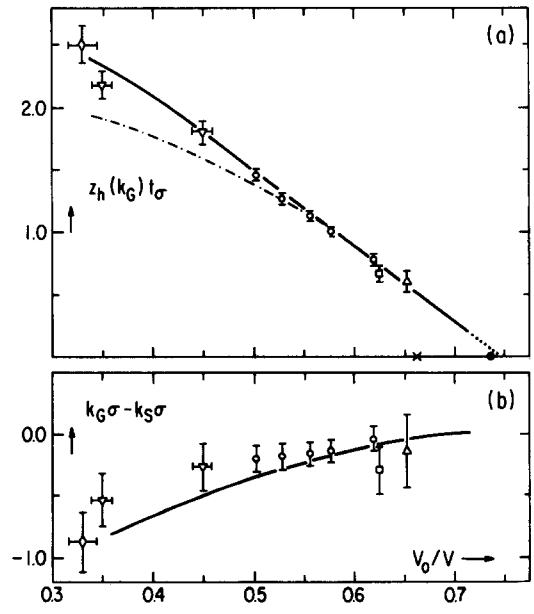

Fig. 3. $z_h(k_G)\, t_\sigma$ (–) and $\omega_H(k_G)\, t_\sigma$ (– • –) (a) and $k_G\sigma - k_S\sigma$ (b) as a function of V_0/V. Experimental data are for He (◇) [7]; Kr (▽) (σ = 3.59 Å) [10]; Ar (○) [9], Ar (□) σ = 3.46Å [3] and Rb (△) σ = 4.44 Å [4]. (•) is the reduced melting and (×) the reduced solidification density of a hard-sphere system and of Ar at 120 K.

eq. (5) applies. As an example, for $V_0/V = 0.625$, the various contributions on the right-hand side of eq. (5) are illustrated in fig. 2b. There we see that $z_h(k)$ oscillates around $z_D(k) \approx D_E k^2$ and that $S(k)$ causes a minimum in $z_h(k)$ at k_G. The oscillations are too large, however, and are considerably corrected by the dynamic factor $d(k)$, thus leading to a result which is close to $z_h(k)$ (and $\omega_H(k)$), at least as long as $kl_E < 1$. We note that $d(k)$ in eq. (5) is also needed to obtain the correct phase of $z_h(k)$, since $k^2/S(k)$ alone and $z_h(k)$ become increasingly out of phase for $k > k_G$. In addition, the remarkably linear behavior of $z_h(k_G) = \omega_H(k_G)$ for $0.52 \lesssim V_0/V \lesssim 0.70$ (where 0.70 is the maximum density for which we know the $S(k)$ for the – then undercooled – hard-sphere fluid) can only be explained using all factors in eq. (5). For decreasing densities $0.52 \gtrsim V_0/V \gtrsim 0.30$, the de Gennes minimum shifts more and more to $k_G l_E = 1$, so that eq. (5) for $z_h(k)$ becomes increasingly bad when $k \approx k_G$. Yet, the equation still gives correctly the increasing flattening out of the de Gennes minimum and its ultimate disappearance for $V_0/V \lesssim 0.3$, where $S(k_S)$ is not

longer high enough to produce a minimum in $z_h(k)$. It still causes, however, a noticeable minimum in $z_h - z_D$ at $k \approx k_s$ (compare figs. 1a and 2a for $k\sigma \approx 2\pi$).

Like for $kl_E \lesssim 1$, with increasing $kl_E \gtrsim 1$ oscillations of $z_h(k)$ around $z_D(k)$ are determined for all densities by the relative importance of those of $S(k)$ around 1 and Λ_k around Λ_∞. In fact, the oscillations of $z_h(k)$ around $z_D(k)$ first decrease but then increase again. While this decrease is due to a destructive interference of $S(k)$ and Λ_k (or $d(k)$), the increase for larger k is due to Λ_k alone, since then $S(k) \ll d(k)$. Thus for sufficiently large k and for *all* densities, the oscillations in $z_h(k)$ have the same phase, viz. that of $d(k)$, as shown in fig. 2 up to $k\sigma = 60$.

Although less prominently, the above sketched behavior of $z_h(k)$ is also present in $\omega_H(k)$ (cf. figs. 1 and 2). A similar interference effect between $S(k)$ and Λ_k explains the peculiar behavior of the strength of the heat mode $A_h(k)$, as illustrated in fig. 4 of ref. [2]. Furthermore, we find that this effect also appears in the behavior of $S(k, 0)$, the top value of $S(k, \omega)$, as a function of k.

As to a comparison of our calculations with recent hard-sphere MD data [5,6], we find that the heat mode eigenvalue $z_h(k)$ determined from eqs. (1) and (4) with $N = 11$, is not noticeably different from the heat mode eigenvalue determined by Alley and Alder [5] from hydrodynamic equations with k-dependent thermodynamic and transport coefficients derived from computer simulation data for $V_0/V = 0.625$ and $0 \leqslant k\sigma \leqslant 20$. We remark, however, that for values of k such that kl_E becomes significantly larger than 1 (i.e., $k\sigma$ significantly larger than 20), at least six modes are needed. Then, such a generalized hydrodynamic description is no longer possible.

For a comparison of our theoretical results with real fluid data, we have to deduce $\omega_H(k)$ and $z_h(k)$ from the experimental $S(k, \omega)$ as well as to define an equivalent hard-sphere fluid. While $\omega_H(k)$ can be deduced directly from $S(k, \omega)$ data for He, Kr, Ar and Rb, $z_h(k)$ has so far only been obtained for Ar at 120 K by a fit of $S(k, \omega)$ with three lorentzians [8]. An equivalent hard-sphere fluid can be defined by taking the mass of the hard spheres in the fluid equal to that of the real fluid particles and fixing their diameter by a comparison of the $S(k)$ of both fluids (cf. refs. [1,2]). Proceeding in this manner, we find that the results for ω_H of He, Kr and Rb as well as for ω_H and z_h for Ar as a function of k are in general consistent with those found for equivalent hard-sphere fluids (cf. figs. 1 and 3). There are, however, systematic deviations, that can be attributed, it seems, to differences in the interparticle potentials. First, for $k\sigma \lesssim 4$ the $z_h(k)$ for liquid argon [8,9] and computer simulated Lennard-Jones fluids [13] on the one hand differ from those obtained from the Enskog theory and simulated repulsive Lennard-Jones fluids [13] on the other hand (cf. figs. 1b and 1c). This is consistent with eq. (5) and the difference in $S(k)$ for the two cases. The same may obtain for krypton [14], where a similar discrepancy between experiment and hard-sphere theory has been observed [10]. Second, while for Ar, $\omega_H(k) = z_h(k)$, within the present experimental accuracy for all observed k, i.e., $k\sigma \lesssim 14$ (cf. figs. 1b and 1c), there is a noticeable difference between these two quantities for hard spheres for $k\sigma \gtrsim 8$, according to our theory. This difference appears to be related to the fact that the contributions of the sound modes to $S(k, \omega)$ are more concentrated near $\omega = 0$ for fluids consisting of particles interacting with a purely repulsive potential, as in a hard-sphere fluid, than with a Lennard-Jones potential, as in Ar (see ref. [13]). A similar situation may obtain for helium (cf. fig. 1a).

In conclusion, we note that like for hard spheres, the $z_h(k_G)$ for argon at 120 K and five densities lie on a straight line, that extrapolates to just beyond the melting density of the solid phase. Moreover, reduction of these argon data to those of equivalent hard-sphere gases, brings the five argon points all on the straight line obtained from the Enskog theory for hard spheres, discussed above, and also makes the reduced melting densities of the ordered phases of Ar and hard spheres coincide at $V_0/V = 0.735$. In addition, also other data for argon as well as for helium, krypton and rubidium, when similarly reduced, all lie on the same Enskog theory line (cf. fig. 3), which extrapolates to zero for $V_0/V = 0.745$. One could wonder whether the smallness of $z_h(k_G)$ near the reduced melting density of Ar and hard spheres is connected with the end of the existence of an undercooled fluid state.

References

[1] I.M. de Schepper and E.G.D. Cohen, Phys. Rev. A22 (1980) 287.
[2] I.M. de Schepper and E.G.D. Cohen, J. Stat. Phys. 27 (1982) 223.
[3] K. Sköld, J.M. Rowe, G. Ostrowski and P.D. Randolph, Phys. Rev. A6 (1972) 1107.
[4] J.R.D. Copley and J.M. Rowe, Phys. Rev. A9 (1974) 1656.
[5] W.E. Alley and B.J. Alder, Phys. Rev. A27 (1983) 3158.
[6] W.E. Alley, B.J. Alder and S. Yip, Phys. Rev. A27 (1983) 3174.
[7] A.D.B. Woods, E.C. Svensson and P. Martel, Can. J. Phys. 56 (1978) 302.
[8] I.M. de Schepper, P. Verkerk, A.A. van Well and L.A. de Graaf, Phys. Rev. Lett. 50 (1983) 974.
[9] A.A. van Well, P. Verkerk and L.A. de Graaf, IRI report 132-82-07;
A.A. van Well, P. Verkerk, L.A. de Graaf, J.-B. Suck and J.R.D. Copley, to be published.
[10] P.A. Egelstaff, W. Glaser, D. Litchinsky, E. Schneider and J.-B. Suck, Phys. Rev. A27 (1983) 1106.
[11] I.M. de Schepper, M.H. Ernst and E.G.D. Cohen, J. Stat. Phys. 25 (1981) 321.
[12] V.F. Sears, Phys. Rev. A5 (1972) 452.
[13] I.M. de Schepper, J.C. van Rijs, A.A. van Well, P. Verkerk, L.A. de Graaf and C. Bruin, Phys. Rev. A (March 1984).
[14] J.J. Ullo and S. Yip, preprint (1984).